Electronic Supplementary Material (ESI) for Journal of Materials Chemistry A.

Highly Efficient Inverted Perovskite Solar Cells Based on Self−assembled Graphene Derivatives

Xuewen Yin[1], Yu Zhou[1], Jianhua Han[1], Hui Nan[1], Meiqian Tai[1], Youchen Gu[1], Jianbao Li[2,1], Hong Lin[1*]

[1]State Key Laboratory of New Ceramics & Fine Processing, School of Materials Science and Engineering, Tsinghua University, Beijing 100084, P. R. China.

[2]Key Laboratory of Ministry of Education for Advanced Materials in Tropical Island Resources, Materials and Chemical Engineering Institute, Hainan University, Haikou 570228, China

E−mail: hong-lin@tsinghua.edu.cn

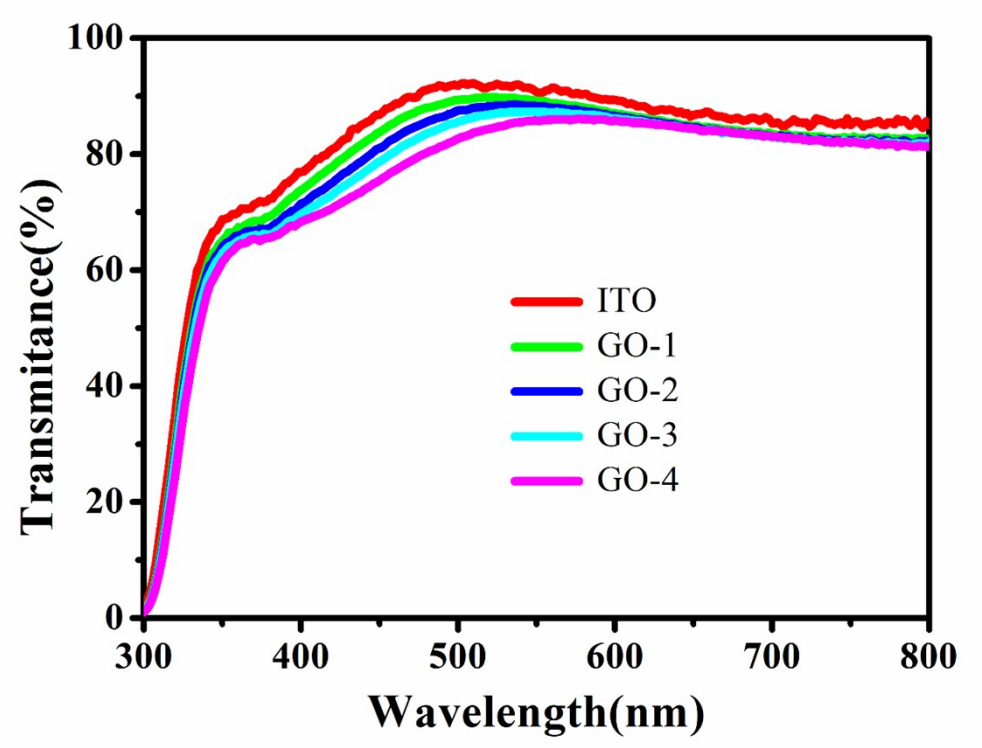

Figure S1. Transmittance spectra of ITO and substrates with GO−n films.

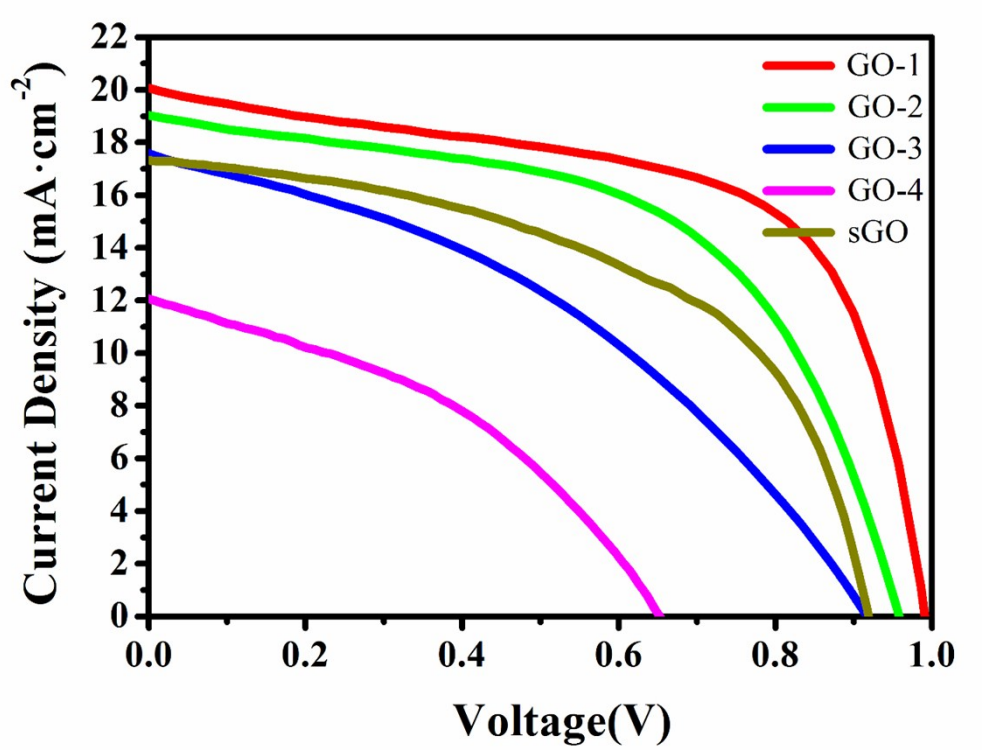

Figure S2. *J*−*V* curves of devices based on GO−n and sGO HTLs.

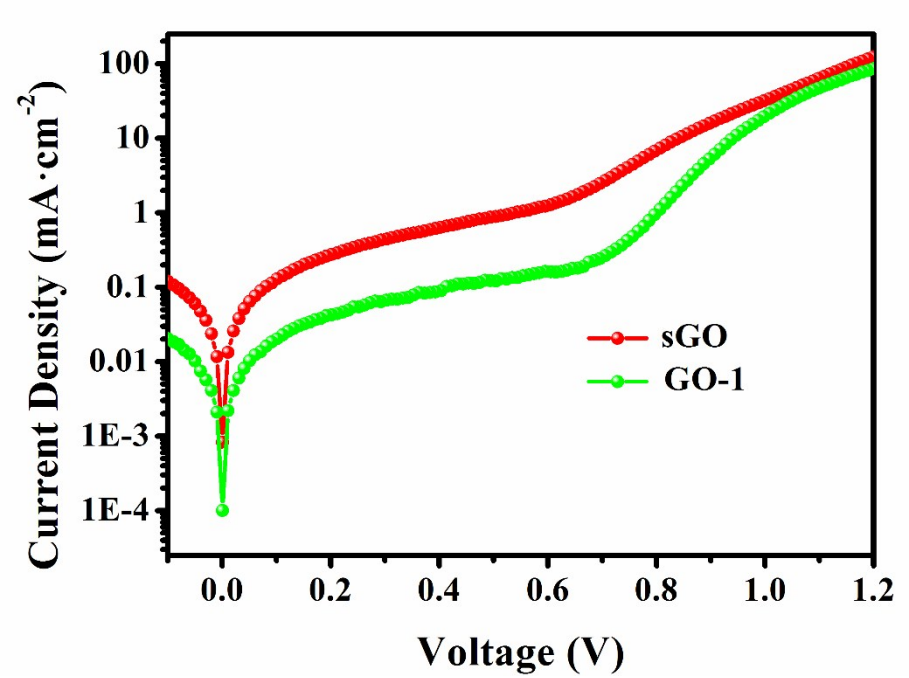

Figure S3. Dark $J-V$ curves of devices based on GO−1 and sGO HTLs.

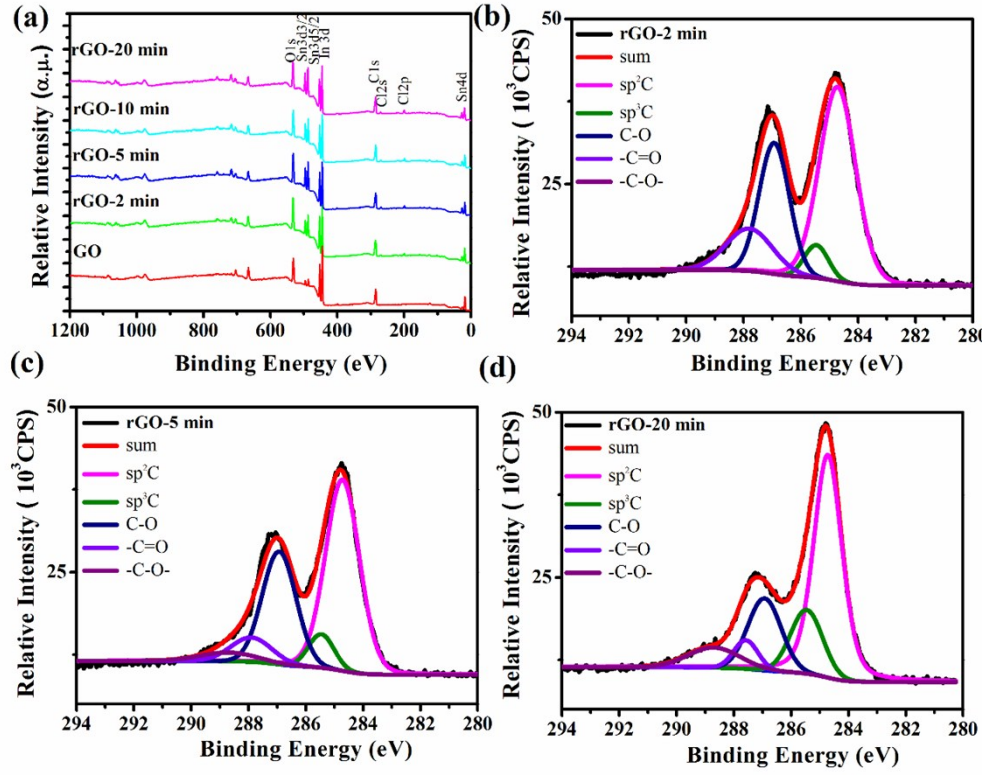

Figure S4. (a) Wide survey XPS spectra, (b−d) Deconvolution of C1s XPS spectra of rGO films on ITO with different reduction time.

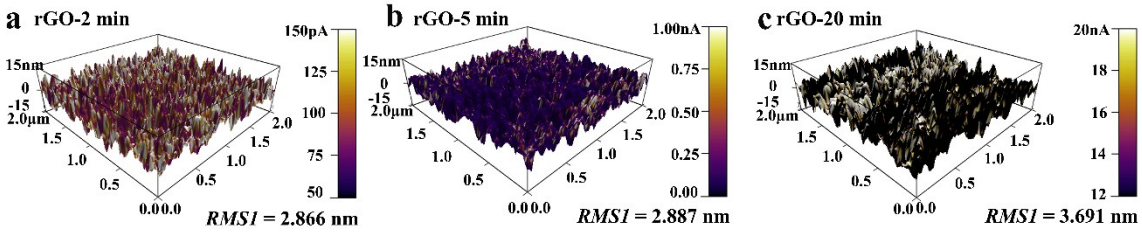

Figure S5. The 3D−AFM height images with current mapping images (color represent) of GO or rGO on ITO under the bias of 4 V. The scale bar represents the current detected by the contacted probe. (a. rGO−2 min; b. rGO−5 min; c. rGO−20 min)

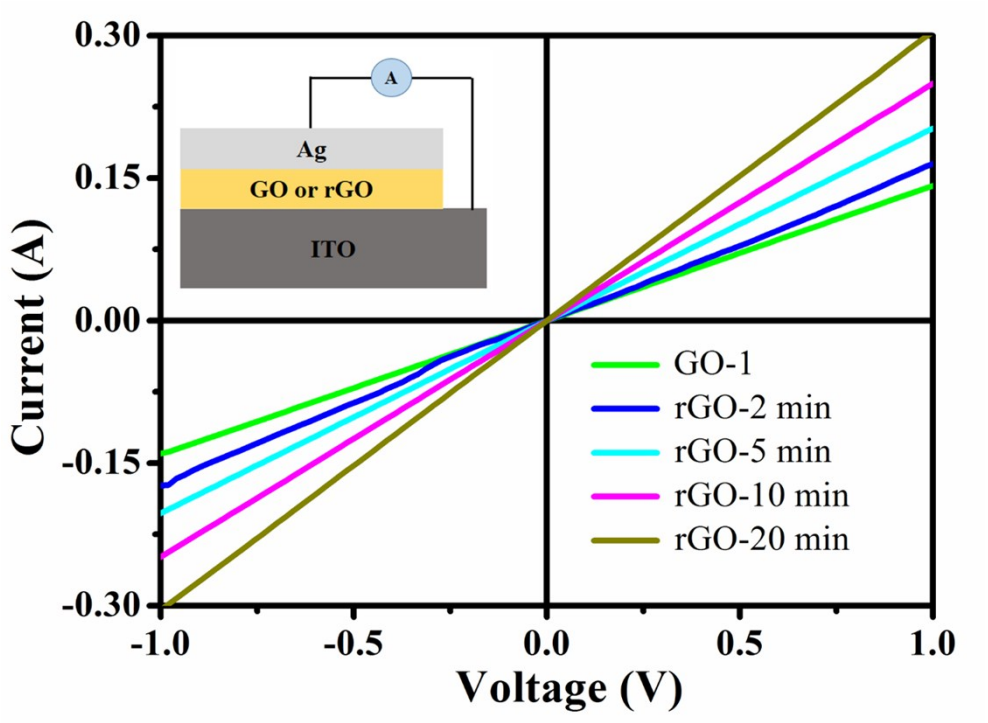

Figure S6. Current–voltage curves, obtained by linear−sweep voltammetry, of GO−1 and r−GO films.

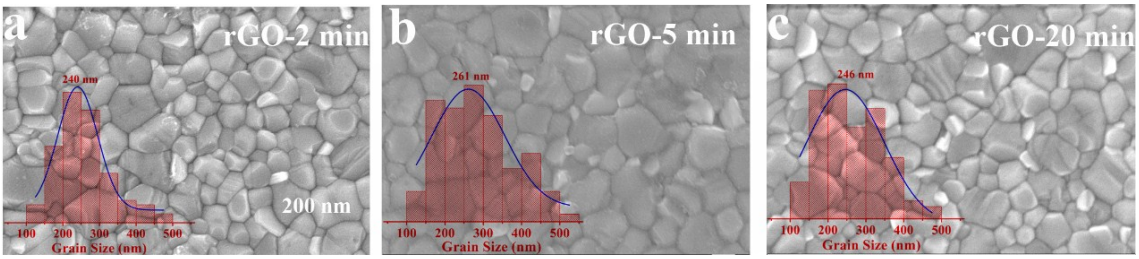

Figure S7. SEM images of perovskites on rGO films. (Inset: Statistical distributions and their Gaussian fitting (solid lines) of the perovskite grain sizes determined from the SEM images. a. rGO−2 min; b. rGO−5 min; c. rGO−20 min)

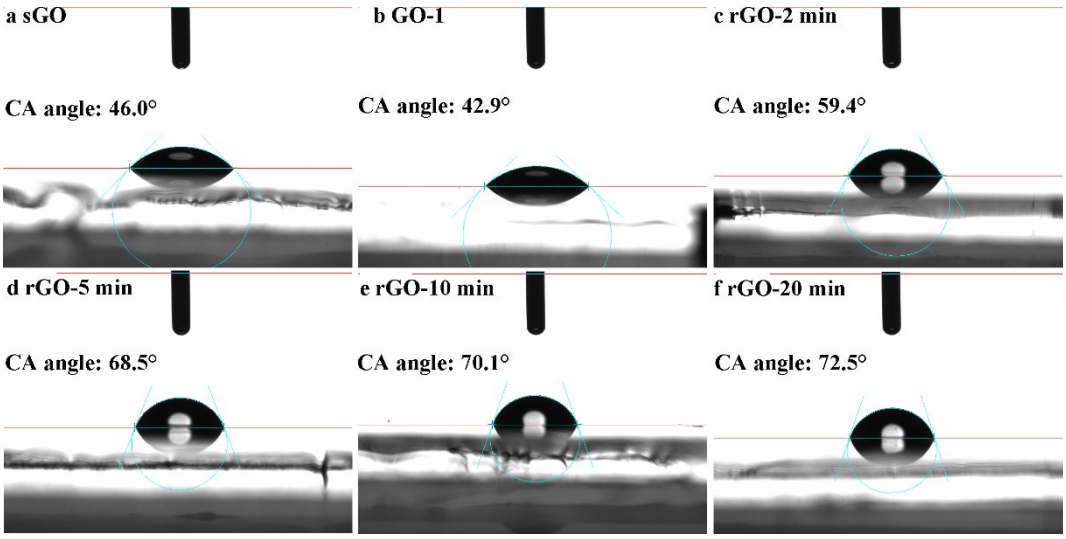

Figure S8. The contact angle images of water on different HTLs. (a. sGO; b. GO−1; c. rGO−2 min; d. rGO−5 min; e. rGO−20 min; f. rGO−20 min.)

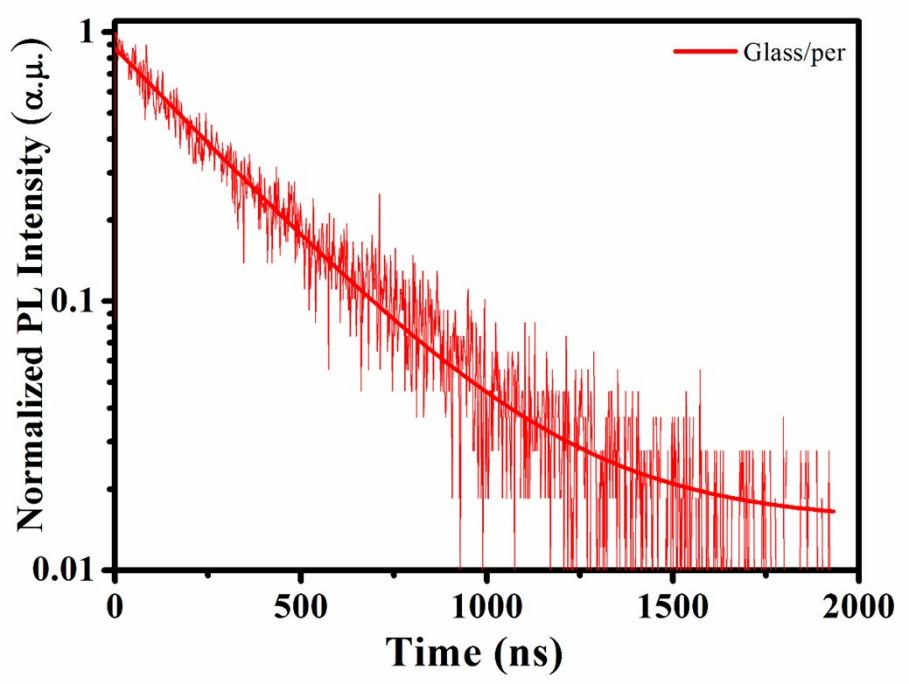

Figure S9. PL decay time spectrum of glass/perovskite.

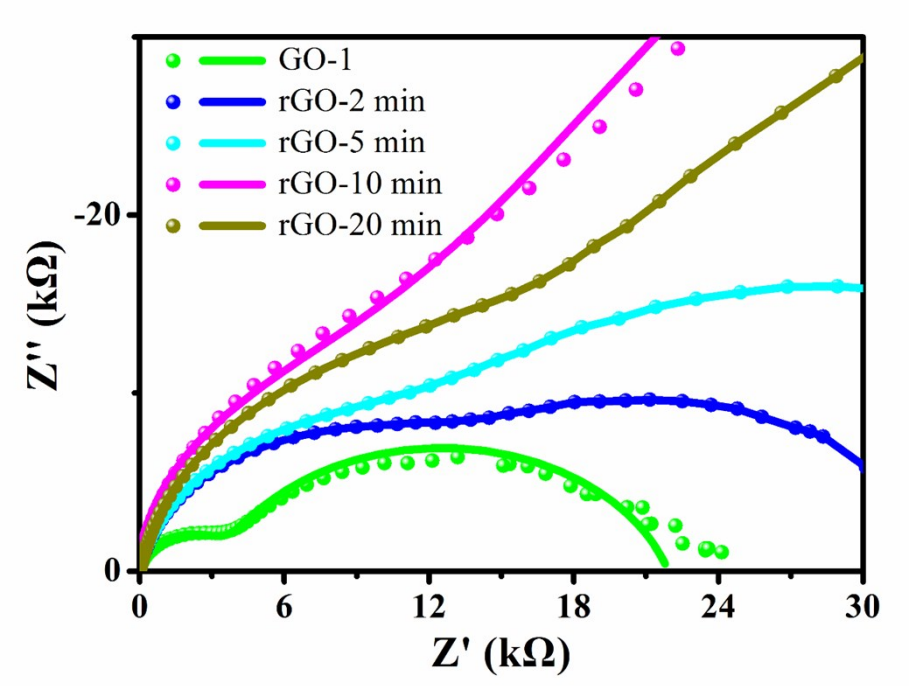

Figure S10. Enlarge figure of EIS Nyquist plots obtained under dark condition at −0.7 V bias voltages of devices with different HTLs.

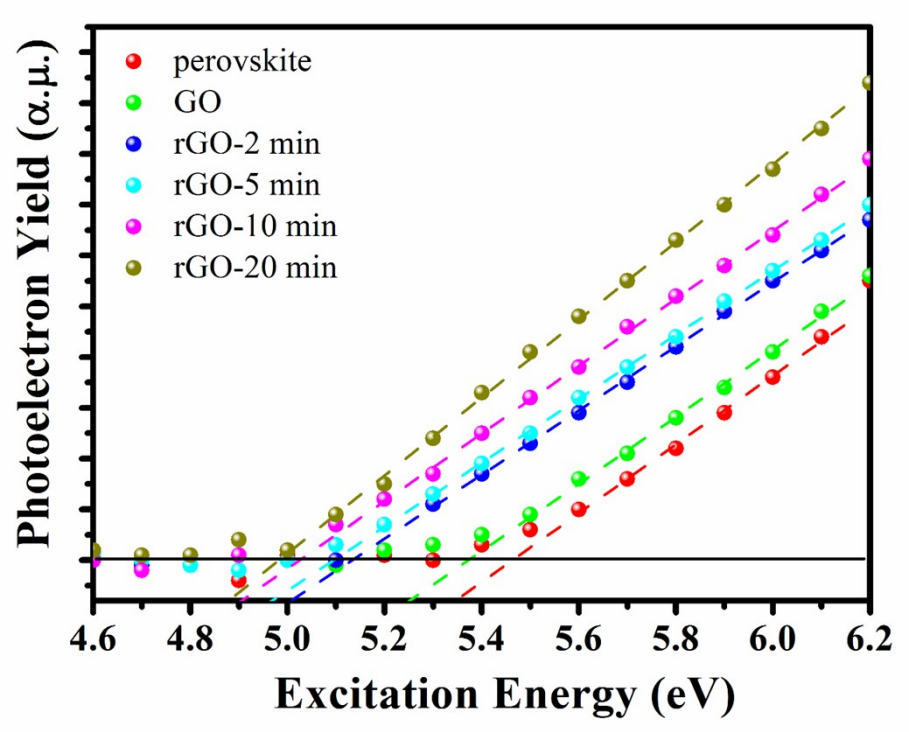

Figure S11. Ultraviolet photoelectron emission spectra of perovskite, GO and rGO films. The black line represents a regression analysis of the measured data.

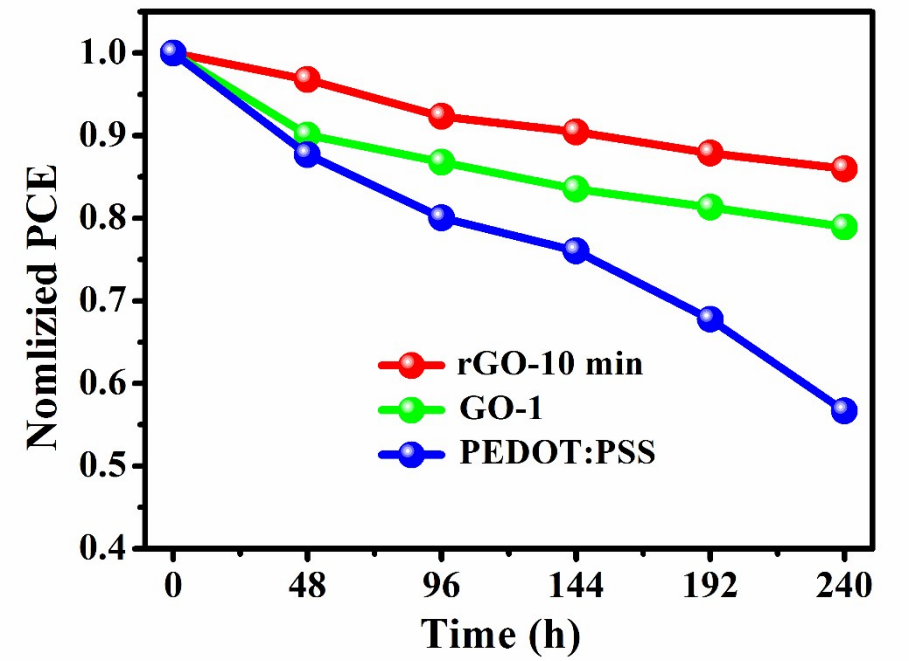

Figure S12. Evolution in normalized PCE values of devices based on PDEOT:PSS, GO−1 and rGO−10 min without encapsulation and stored in ambient condition with 40% ±5% humidity.

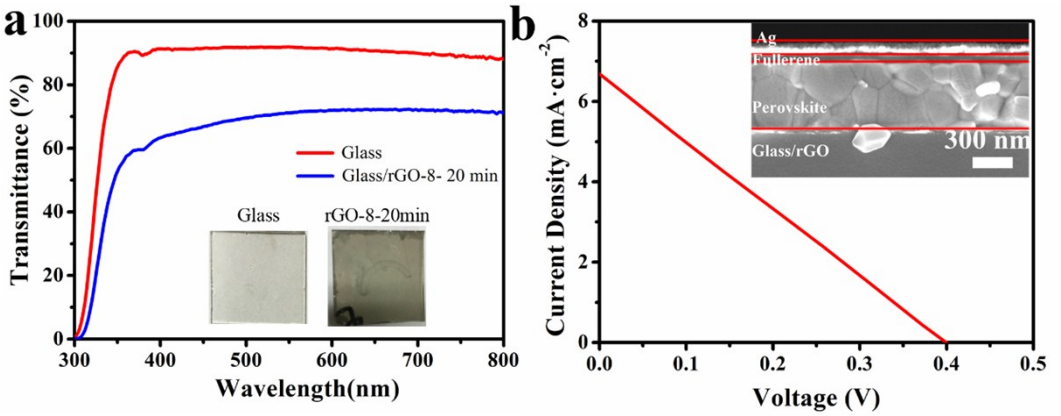

Figure S13. (a) Transmittance spectra of glass and glass/rGO−8−20 min. (Inset: images of glass and glass/rGO−8−20 min (glass/rGO−8−20 min means rGO films obtained by processing GO−8 films prepared by LbL method with 8 cycles together with reduction time of 20 min as shown in experimental section.)) (b) The $J-V$ curve of the device based on rGO electrode. (Inset: the cross−sectional SEM image of the device.)

Table S1. Root−mean−square of current (*RMS2*) obtained by C−AFM measurement

ID	*RMS2* [1] (nA)
ITO	17.718
GO−1	0.091
rGO−2 min	0.099
rGO−5 min	1.025
rGO−10 min	9.556
rGO−20 min	10.129

[1]*RMS2*: root−mean−square of surface current

Table S2. Photovoltaic parameters of the devices based on different HTLs

ID	J_{sc} (mA·cm^{-2})	V_{oc}(V)	FF (%)	PCE (%)
GO−1	19.95	0.986	62.36	12.26
rGO−2 min	20.59	1.071	62.31	13.75
rGO−5 min	21.43	1.071	66.37	15.24
rGO−10 min	21.46	1.060	71.61	16.28
rGO−20 min	20.02	1.031	66.23	13.67

Table S3. The dynamic decay time parameters of the perovskites with different substrates

	τ_1（ns）	τ_2（ns）
Glass/perovskite	/	298.89
ITO/GO−1/perovskite	1.59	20.16
ITO/ rGO−2 min /perovskite	1.78	21.42
ITO/ rGO−5 min /perovskite	2.27	24.17
ITO/ rGO−10 min /perovskite	4.04	25.58
ITO/ rGO−10 min /perovskite	4.20	27.59

Table S4. EIS parameters of devices with different ETLs by fitting EIS Nyquist plots

	R_s (Ω)	R_{ct} (Ω)	CPE1−T	CPE1−P	R_{rec} (Ω)	CPE2−T	CPE2−P
GO−1	10.38	4173	1.26E−08	0.94	18047	5.61E−07	0.77
rGO−2 min	17.60	9538	4.72E−09	1.01	24726	3.58E−07	0.66
rGO−5 min	17.83	11036	6.04E−09	0.99	40330	2.15E−07	0.71
rGO−10 min	16.98	21558	5.15E−09	1.00	230660	7.32E−08	0.79
rGO−20 min	18.55	22160	8.17E−09	0.96	91291	7.93E−08	0.84

Table S5 Summary on the performances and preparation methods of solution processed graphene−based inverted organic−inorganic hybrid PSCs including the present devices. The word “non” means the parameter was not presented in the literature.

Device configuration (Bold font: HTL)	**V_{oc} (V)**	**J_{sc} (mA/cm^2)**	**FF (%)**	**PCE (%)**	**Preparation methods**	**Reductant**	**Reference**
ITO/**LBL GO**/mixed perovskite/PCBM/BCP/Ag	0.986	19.95	62.36	12.26	Layer by Layer method	$SnCl_2$/ethanol	**This work**
ITO/**LBL rGO**/mixed perovskite/PCBM/BCP/Ag	1.060	21.46	71.61	16.28			
ITO/**GO**/$MAPbI_3$/PCBM/BCP/Ag	0.89	10.70	37.61	3.58	Spin−coating	Hydrazinobenzenesulfonic Acid hemihydrate	1
ITO/**RGO**/$MAPbI_3$/PCBM/BCP/Ag	0.95	14.81	71.13	9.95			
ITO/**GO**/$MAPbI_3$/PCBM/LiF/Ag	0.85	12.74	60.19	6.55	Spin−coating	Non	2
ITO/**GO−PEDOT:PSS**/$MAPbI_3$/PCBM/LiF/Ag	0.84	15.75	73.56	9.74			
ITO/**PRGO**/$MAPbI_3$/PCBM/BCP/Ag	0.94	15.61	66.08	9.70	Spin−coating	Polyacrylonitrile	3
FTO/**GO**/perovskite/GO−Li/Al	0.89	13.2	0.60	7.1	Spin−coating	Non	4
FTO/**GO**/perovskite/Ti−based sol/GO−Li/Al	0.91	15.6	0.72	10.2			
ITO/**GO**/$CH_3NH_3PbI_{3-x}Cl_x$/PCBM/ZnO/Al	0.99	15.59	72	11.11	Spin−coating	Non	5
ITO/**GO−PEDOT:PSS**/$MAPbI_3$/PCBM/LiF/Al	0.93	13.5	0.69	8.7	Spin−coating	Non	6
ITO/**GGO−PEDOT:PSS**/$MAPbI_3$/PCBM/LiF/Al	1.05	17.6	0.69	12.8			

FTO/**NGONR**/$MAPbI_3$/ZnO NPs/Al	1.00	17.93	72.16	12.94	Spin−coating	Non	7
ITO/**MHGO**/$MAPbI_3$/PCBM/BCP/Ag ITO/**MFGO**/$MAPbI_3$/PCBM/BCP/Ag	0.86 1.01	16.7 19.1	72.5 76.2	10.5 14.7	Spin−coating	Phenylhydrazine 4(trifluoromethyl)phenylhydrazine	8
ITO/ **GO−PEDOT:PSS**/$MAPbI_3$/PCBM/BCP/Ag	0.90	20.01	0.79	14.20	Spin−coating	Non	9
ITO/**PEDOT:PSS−GO**/$CH_3NH_3PbI_{3-x}Cl_x$/PCBM/sBphen/Ag ITO/**PEDOT:PSS−GO:NH$_3$**/$CH_3NH_3PbI_{3-x}Cl_x$/PCBM/sBphen/Ag	0.96 1.03	21.80 22.06	69.0 71.0	14.42 16.11	Spin−coating	Non	10
ITO/**GO**/$MAPbI_3$/PCBM/Ag ITO/**rGO−NH**/$MAPbI_3$/PCBM/Ag ITO/**rGO−BH**/$MAPbI_3$/PCBM/Ag ITO/**rGO−HBS**/$MAPbI_3$/PCBM/Ag	0.943 0.963 0.965 0.962	19.5 21.3 21.4 22.1	0.751 0.787 0.742 0.770	13.8 16.0 15.3 16.4	Spin−coating	/ Hydrazine $NaBH_4$ 4−hydrazinobenzenesulfonic acid	11
ITO/**rGO**/$MAPbI_3$/PCBM /BCP/Ag ITO/**r−GO/PTAA**/$MAPbI_3$/PCBM/BCP/Ag	1.07 1.09	19.4 20.3	74.2 77.7	15.4 17.2	Spin−coating	Thermal reduction (100−200°C)	12

References

1. Yeo, J, Kang, R, Lee, S, Jeon, Y, Myoung, N, Lee, C, Kim, D, Yun, J, Seo, Y, Kim, S, Na, S, Highly efficient and stable planar perovskite solar cells with reduced graphene oxide nanosheets as electrode interlayer. *Nano Energy* **2015**, 12, 96−104.
2. Lee, D, Na, S, Kim, S, Graphene oxide/PEDOT:PSS composite hole transport layer for efficient and stable planar heterojunction perovskite solar cells. *Nanoscale* **2016**, 8, 1513−1522.
3. Jung, C, Noh, Y, Bae, J, Yu, J, Hwang, I, Shin, J, Shin, K, Lee, J, Choi, J, Na, S, Polyacrylonitrile−grafted reduced graphene oxide hybrid: an all−round and efficient hole−extraction material for organic and inorganic−organic hybrid photovoltaics. *Nano Energy* **2017**, 31, 19−27.
4. Nouri, E, Mohammadi, MR, Lianos, P, Inverted perovskite solar cells based on lithium−functionalized graphene oxide as an electron−transporting layer. *Chem. Commun.* **2017**, 53 (1), 163−1633.
5. Wu, Z, Bai, S, Xiang, J, Yuan, Z, Yang, Y, Cui, W, Gao, X, Liu, Z, Jin, Y, Sun, B, Efficient planar heterojunction perovskite solar cells employing graphene oxide as hole conductor. *Nanoscale* **2014**, 6 (18), 10505.
6. Giuri, A, Masi, S, Colella, S, Kovtun, A, Dell'Elce, S, Treossi, E, Liscio, A, Esposito Corcione, C, Rizzo, A, Listorti, A, Cooperative effect of GO and Glucose on PEDOT:PSS for high V_{oc} and hysteresis−free solution−processed perovskite solar cells. *Adv. Func. Mater.* **2016**, 26 (38), 6985−6994.

7. Kim, J, Mat Teridi, MA, Mohd Yusoff, ARB, Jang, J, Stable and null current hysteresis perovskite solar cells based nitrogen doped graphene oxide nanoribbons hole transport layer. *Sci. Rep.* **2016**, 6, 27773.

8. Yeo, J, Lee, C, Jang, D, Lee, S, Jo, SM, Joh, H, Kim, D, Reduced graphene oxide−assisted crystallization of perovskite via solution−process for efficient and stable planar solar cells with module−scales. *Nano Energy* **2016**, 30, 667−676.

9. Niu, J, Yang, D, Ren, X, Yang, Z, Liu, Y, Zhu, X, Zhao, W, Liu, SF, Graphene−oxide doped PEDOT:PSS as a superior hole transport material for high−efficiency perovskite solar cell. *Org. Electron.* **2017**, 48, 165−171.

10. Feng, S, Yang, Y, Li, M, Wang, J, Cheng, Z, Li, J, Ji, G, Yin, G, Song, F, Wang, Z, Li, J, Gao, X, High−performance perovskite solar cells engineered by an ammonia modified graphene oxide interfacial layer. *ACS Appl. Mater. Interface* **2016**, 8 (23), 14503−14512.

11. Jokar, E, Huang, ZY, Narra, S, Wang, C, Kattoor, V, Chung, C, Diau, EW, Anomalous charge−extraction behavior for graphene−oxide (GO) and reduced graphene−oxide (RGO) films as efficient p−contact layers for high−performance perovskite solar cells. *Adv. Energy Mater.* **2017**, 1701640.

12. Zhou, Z, Li, X, Cai, M, Xie, F, Wu, Y, Lan, Z, Yang, X, Qiang, Y, Islam, A, Han, L, Stable inverted planar perovskite solar cells with low−temperature−processed hole−transport bilayer. *Adv. Energy Mater.* **2017**, 1700763.